



## Voltage Regulation of a Negative Output Luo Converter Using a PD-PI Type Sliding Mode Current Controller

A. Goudarzian\*, A. Khosravi

Department of Electrical Engineering, Faculty of Engineering, Shahrekord Branch, Islamic Azad University, Shahrekord, Iran

### PAPER INFO

#### Paper history:

Received 19 September 2018

Received in revised form 19 November 2017

Accepted 03 January 2019

#### Keywords:

Switching Converter

Negative Output Luo Converter

PD-PI Type Sliding Surface

Control Design

### ABSTRACT

This paper describes a new design for direct sliding mode method with a high switching frequency using the PD-PI type sliding surface applied to a negative output Luo converter worked in continuous current mode for applications required constant power source such as aerospace applications, medical equipment and etc. Because of the output power and line changes, the converter model is also nonlinear and time varying. In addition, losses dissipation and voltage drops caused a deviation between the theoretical and actual output voltage of this converter. For improvement of the converter performance along with the current and voltage regulations, a nonlinear controller is required. This suggested controller is proper to inherently variable structure of the converter and can cope with nonlinearities associated with its model. The goal is to ensure a satisfactory response for the converter. The practical results showed that the proposed strategy helps to eliminate the voltage error along with continuous current operation of the converter in very light loads and high switching frequency in different operating points.

doi: 10.5829/ije.2019.32.02b.13

## 1. INTRODUCTION

In recent years, power converters are commonly employed in power supplies and industrial applications [1]. Theoretically, conventional topologies such as buck-boost, Sepic, Zeta, Cuk could be employed for voltage increment. However, effects of switches, diodes, and the consequence of resistances of passive elements and losses limit the practical voltage gain of the aforementioned converters. Moreover, duty ratio of the converters will tremendously increase by increment of the output voltage. This terribly large duty ratio leads to relatively high switching losses and severe reverse recovery crisis [2]. In two last decades, the voltage lift method has been well applied for design of power converters [3]. In addition, the super lift technique geometrically enhances the voltage gain, whereas the negative output Luo converter (NOLC) does the same operation. NOLC has a high voltage gain, high power density and high efficiency. For similar conditions, the switching stress of this converter is less than the

switching stress of other conventional converters. It is an extremely useful feature to reduce switching losses. Hence, NOLC is used for this study. In practice, the voltage gain of a NOLC is dependent to parametric resistances of power circuit components and operating point. Hence, a controller is needed for adjustment of the magnitude of the output voltage with respect to its reference signal and guarantee the converter stability. From control viewpoint, the boost converters have a non-minimum phase and time-varying structure. The non-minimum phase converters have a slow dynamical response and small stability margins [4]. Hence, control of a NOLC is more complicated compared with minimum phase systems.

Small-signal analysis is presented for switching converters in literature [5, 6]. However, the duty ratio of a converter is restricted in interval of 0 and 1. The classical controllers cannot meet the dynamical performance of a non-linear converter in saturated region. Commonly, power converters are exposed to load and line variations. These oscillations may affect the

\*Corresponding Author Email: [alireza9071@gmail.com](mailto:alireza9071@gmail.com) (A. Goudarzian)

stability of converters. It may challenge the quality, performance and stability of power systems. Therefore, a voltage regulator is required. Peak current mode method (PCM) is a type of nonlinear methods which is designed for converters [7]. However, the problem of PCM is presence of an exterior ramp signal. Consequently, the current cannot exactly reach to its desired level. An adaptive backstepping controller is proposed for a POESLLC by Abjadi et al. [8]. However, this controller needs to precise knowledge of all parameters of the converter, excepting load. Therefore, the cost increases and productivity is reduced. Also, stability analysis and construction of fuzzy controllers are reported for converters, aiming to enhance large signal characteristics [9]. However, there is no systematic method for selection of coefficients of fuzzy controllers.

In the last decade, sliding mode controller (SMC) has been widely regarded for variable structure systems [10, 11]. Two major methods exist to implement an SMC for a switching power converter, namely the indirect and direct SMC techniques. In indirect method, the control law of a converter is obtained using the equivalent control concept [12]. However, the designed sliding variable is not bounded and the system response will be deteriorated. In direct method, the switching function is directly achieved using instantaneous trajectories of the SMC. One method to generate the pulse signals for the converter is to modulate the sliding plane within a parabolic modulator (PM) with variable bandwidth [13] or a constant bandwidth hysteresis modulator (HM) [14]. However, the proposed approaches in literature [13, 14] are used for minimum phase systems. For stabilization of a non-minimum phase converter, sliding mode current control (SMCC) method should be utilized. Mamarelis et al. [15] proposes a simple SMCC for boost and Sepic converters. Although the main objective is the voltage regulation, but any output feedback was not applied to generate the reference input current. So they are weak against large load uncertainties. Furthermore, switching frequency of power electronics systems with traditional direct SMCC will be constrained, due to time delays of command circuits, analogue to analogue conversions for isolated sensors and also, parametric resistances effects of power circuits, limited bandwidth of analogue devices and etc. For power converters, low switching frequency leads to inductor core saturation, noise, large voltage ripple and etc. In addition, implementation of a simple SMCC is proposed in literature [16, 17] using digital processors. However, digital control has a serious drawbacks, which decreases sampling frequency. By observing the reported data in literature [16, 17], it is found that the converter frequency is about 10 KHz for all the tests, provided by the authors. However, the frequency must be larger than the audible frequency i.e.  $f_s > 20 \text{ KHz}$ . It is recommended for low power converters to work in interval of [20 200] KHz.

In view of the aforementioned discussions, this research presents a new direct SMCC controller via PD-PI type sliding surface. This solution can resolve the problems discussed in the above associated literature [11-17]. The proposed structure is presented in Figure 1. It is consisted of two loops; i) an inner loop through a proportional-integral (PI) controller. It is used to adjust the voltage and alleviate the voltage error, and ii) an outer loop via a proportional-derivative (PD) controller. It should be used for stabilizing the converter dynamics, minimizing inrush current and enhancing the switching frequency. By employing a PD compensator in the SMCC, derivative of the sliding variable (S) will be dependent to the impulse function. Therefore, the sliding surface derivative will be converged to infinite and high switching frequency operation will be achieved, despite of having a practical large hysteresis bandwidth. Other features of the controller, such as the steady state and dynamic performances are investigated in the paper. Theoretically, it is demonstrated that the utilization of a PD controller effectively enhances the switching frequency and practical tests are performed to confirm the validity of the suggested method

The contents of the paper are as follows. In section 2, a comparison between NOLC and other converters is preformed. design, development and system stability of the proposed PD-PI SMCC for a NOLC are investigated in section 3. The practical results are represented in section 4 and the conclusions are shown in section 5.

## 2. COMPARISON BETWEEN NOLC AND OTHER CONVERTERS

The NOLC diagram illustrated in Figure 1, and it consists of a semiconductor switch, two diodes, three energy storage elements, resistance and input source. The converter operation investigated in two mode. At the first mode, the switch and diode  $D_1$  are turned on and the diode  $D_2$  is off. At the second mode, switch and diode  $D_1$  are turned off and diode  $D_2$  conducts. The advantages of NOLC compared with other converters is expressed in the following expression.

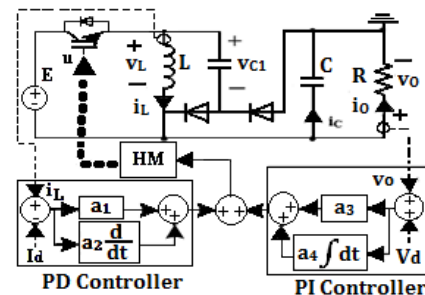


Figure 1. Control scheme of the proposed PD-PI SMC for the NOLC

The switching stress is defined as follows:

$$P_S = V_T I_T \tag{1}$$

where  $P_S$  is switching losses,  $V_T$  is switch voltage drop in ON and OFF instants and  $I_T$  is switch current in ON and OFF instants.  $V_T$  and  $I_T$  are obtained for NOLC as follows:

$$V_T = v_O \tag{2-a}$$

$$I_T = I_{in} = \frac{P_O}{E} \tag{2-b}$$

where  $\Delta v_{C1}$  is the voltage ripple of the middle capacitor and  $P_O$  is output power. By using Equations (1) and (2), the switching losses of the NOLC can be given as follows:

$$P_S = \frac{V_O}{E} P_O = G P_O \tag{3}$$

where  $G = V_O/E$  is the voltage gain. Similarly, the switching stress of buck-boost (BB), Cuk, SEPIC and Zeta converters can be determined as follows:

$$P_S = (G + 1)P_O \quad \text{for BB, Cuk, SEPIC and Zeta} \tag{4}$$

Comparing the switching stress of NOLC as expressed in Equation (3) with Equation (4). It shows that the switching stress of BB, Zeta, Cuk and SEPIC converters extremely increases in high voltage gains. But, the switching losses of the NOLC is less than others despite of increment of the voltage gain, resulting in low switching losses and high efficiency of the NOLC.

## 2. SMCC DESIGN

**2.1. Principles** The operation of a SMCC depicted in Figure 2 for a NOLC. It provides a three-dimensional phase portrait for the inductor current  $i_L$ , output voltage  $v_O$  and sliding variable  $S$ . For any initial operating condition that the sliding variable doesn't start from zero, the state trajectory of the sliding plane is constituted by three regions; namely, the reaching mode, the sliding mode, and the steady mode. In the first region, the state variables are enforced to approach to the sliding variable from any initial conditions. As soon as the sliding surface touches the origin, the state space variables of the converter slide along the sliding variable and approach to their equilibrium points in the second region. Finally, the phase trajectories of the sliding variable are maintained at zero, representing the steady region with no error. The operation of a perfect SMC needs an infinite switching frequency performance of the NOLC. However, in practical applications, the sliding motion of the phase trajectories often introduces the chattering problem at vicinity of the origin. For solving this problem, hysteresis modulation is proposed. However, this method reduces the switching frequency to a limited range.

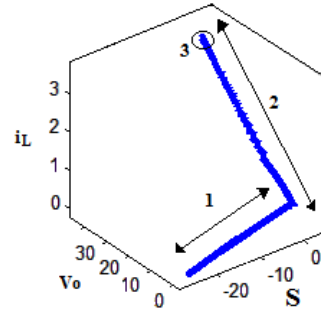


**Figure 2.** The operation of a SMC. Line1: reaching trajectory; Line 2: sliding trajectory; Line 3: steady state region

Also, time delays restrict the frequency of a SMC. One suitable method to reduce the trajectory chattering is directly use of the PD-PI type of SMC within a constant hysteresis bandwidth.

## 2. 2. Closed Loop Analysis of the NOLC with the Proposed Pd-Pi SMC

A PD-PI SMC for a non-minimum phase NOLC is depicted in Figure 1. The reduced order averaging model of a NOLC in CCM can be determined as follows:

$$\begin{cases} \frac{di_L}{dt} = \frac{E}{L} - \frac{(1-u)v_O}{L} \\ \frac{dv_O}{dt} = \frac{(1-u)i_L}{C} - \frac{v_O}{RC} \end{cases} \tag{5}$$

For NOLC, the voltage value of the middle capacitor equals to input voltage for all times. A second order PD-PI type of the sliding variable is chosen as follows:

$$S = a_1 x_1 + a_2 x_2 + a_3 x_3 + a_4 x_4 = a_1 e_1 + a_2 \dot{e}_1 + a_3 e_2 + a_4 \int e_2 dt \tag{6}$$

where  $e_1 = i_L - I_d$  and  $e_2 = v_O - V_d$  are the current and voltage tracking errors, respectively. Also,  $a_1, a_2, a_3$  and  $a_4$  are the parameters of the controller. For the converter, the control law of the SMC is as follows:

$$u = \begin{cases} 1 & \text{for } S < -\varepsilon \\ 0 & \text{for } S > \varepsilon \\ \text{unchanged} & \text{for } -\varepsilon < S < \varepsilon \end{cases} \tag{7}$$

The sliding phase portrait of the controlled system is obtained as follows:

$$a_1 x_1 + a_2 x_2 + a_3 x_3 + a_4 x_4 = 0 \tag{8}$$

Furthermore,  $\dot{e}_1, \ddot{e}_1, e_2, \dot{e}_2$  can be derived as:

$$\begin{cases} \dot{e}_1 = \frac{E}{L} - \frac{(1-u)v_O}{L} \\ \ddot{e}_1 = \frac{u v_O}{L} - \frac{(1-u)v_O}{L} \\ e_2 = v_O - V_d \\ \dot{e}_2 = v_O \end{cases} \tag{9}$$

where  $L, C$  and  $R$  are the inductor, output capacitor and resistance of the NOLC, respectively. Also,  $i_L, v_O, E$  and

u are the inductor current, output voltage, input voltage and switching state of the converter. u is 1 for ON mode and 0 for OFF mode. By using Equations (5)-(9), the time derivative of the designed sliding variable is obtained as follows:

$$\frac{ds}{dt} = k_1 E - k_1(1-u)v_o + k_2 u' v_o - k_2(1-u)v_o' + a_3 v_o' + a_4(v_o - V_d) \quad (10)$$

where

$$k_1 = \frac{a_1}{L}, k_2 = \frac{a_2}{L} \quad (11)$$

For analysis of the system stability, the existence and stability conditions are checked. The first condition was investigated using a Lyapunov function. Let us define Equation (12) as a positive function for the described system:

$$F = \frac{1}{2} S^2 > 0 \quad (12)$$

Differentiating Equation (12) gives:

$$F' = \frac{1}{2L} S(2a_1 E - 2a_1(1-u)v_o + 2a_2 \dot{u} v_o + [2La_3 - 2a_2(1-u)] \left( \frac{(1-u)i_L}{C} - \frac{v_o}{RC} \right) + 2La_4(v_o - V_d)) \quad (13)$$

when  $S > \varepsilon$ , switch is OFF ( $u=0, \dot{u} = -\delta(t)$ ) and Equation (13) is simplified as follows:

$$F' = \frac{1}{2L} S(2a_1 E - 2a_1 v_o - 2a_2 v_o \delta(t) + [2La_3 - 2a_2] \left( \frac{i_L}{C} - \frac{v_o}{RC} \right) + 2La_4(v_o - V_d)) \quad (14)$$

when  $S < -\varepsilon$ , switch is ON ( $u=1, \dot{u} = \delta(t)$ ) and Equation (13) is simplified as follows:

$$F' = \frac{1}{2L} S(2a_1 E + 2a_2 v_o \delta(t) - 2La_3 \frac{v_o}{RC} + 2La_4(v_o - V_d)) \quad (15)$$

By combining Equations (14) and (15), Equation (13) can be expressed as follows:

$$F' = \frac{1}{2L} \left[ S \left( 2a_1 E - 2La_3 \frac{v_o}{RC} + 2La_4(v_o - V_d) - a_1 v_o + [La_3 - a_2] \frac{i_L}{C} + a_2 \frac{v_o}{RC} \right) - |S| \left( a_1 v_o + 2a_2 v_o \delta(t) - [La_3 - a_2] \frac{i_L}{C} - a_2 \frac{v_o}{RC} \right) \right] \rightarrow F' = \frac{1}{2L} |S| \left[ \text{sgn}(S) \left( 2a_1 E - 2La_3 \frac{v_o}{RC} + 2La_4(v_o - V_d) - a_1 v_o + [La_3 - a_2] \frac{i_L}{C} + a_2 \frac{v_o}{RC} \right) - \left( a_1 v_o + 2a_2 v_o \delta(t) - [La_3 - a_2] \frac{i_L}{C} - a_2 \frac{v_o}{RC} \right) \right] \quad (16)$$

The above equation satisfies the following inequality:

$$F' < \frac{1}{2L} |S| \left[ \left| 2a_1 E - 2La_3 \frac{v_o}{RC} + 2La_4(v_o - V_d) - a_1 v_o + [La_3 - a_2] \frac{i_L}{C} + a_2 \frac{v_o}{RC} \right| - a_1 v_o - 2a_2 v_o \delta(t) + [La_3 - a_2] \frac{i_L}{C} + a_2 \frac{v_o}{RC} \right] \quad (17)$$

The following condition ensures that  $F' < 0$ .

$$\left[ 2a_1 E - 2La_3 \frac{v_o}{RC} + 2La_4(v_o - V_d) - a_1 v_o + [La_3 - a_2] \frac{i_L}{C} + a_2 \frac{v_o}{RC} \right] - a_1 v_o - 2a_2 v_o \delta(t) + [La_3 - a_2] \frac{i_L}{C} + a_2 \frac{v_o}{RC} < 0 \quad (18)$$

(18) leads to:

$$0 < a_1 E + La_4(v_o - V_d) + a_2 v_o \delta(t) - La_3 \frac{v_o}{RC} < a_1 v_o - [La_3 - a_2] \frac{i_L}{C} - a_2 \frac{v_o}{RC} + a_2 v_o \delta(t) \quad (19)$$

If the initial conditions are  $v_o(0) \geq 0$  and  $i_L(0) \geq 0$ , the existence conditions will be satisfied and the sliding surface will go to the reaching phase at a finite time. After this region,  $S' \approx 0$  and  $S = 0$ . Also,  $i_L \approx I_d$  and  $S' = I_d' \approx 0$ . Since  $La_3$  and  $La_4$  are very small; thus,  $La_4(v_o - V_d) \approx 0$  and  $a_2 \gg La_3 > 0$ . Also,  $E > 0, v_o > E$  are satisfied for the NOLC, because of its inherent nature; then, if  $i_L > \frac{v_o}{R}$ , Equation (19) is satisfied in a wide range of operating conditions. Since the control law (7) doesn't contain control gain to be adjusted, Equation (19) is predetermined through the controller architecture. For study of the stability condition, the Filippov's technique is used. After the sliding variable reaches to zero, the discontinuous control law (7) can be replaced by a continuous equivalent control signal  $u_{eq}$  which is obtained by solving  $S' = u' = 0$  as:

$$S' = k_1 E - k_1(1-u)v_o + k_2 u' v_o - k_2(1-u)v_o' + a_3 v_o' + a_4(v_o - V_d) = 0 \rightarrow u' = \frac{k_1(1-u)v_o + k_2(1-u)v_o' - k_1 E - a_3 v_o' - a_4(v_o - V_d)}{k_2 v_o} = 0 \rightarrow u_{eq} = \frac{k_1 v_o + k_2 v_o' - k_1 E - a_3 v_o' - a_4(v_o - V_d)}{k_1 v_o + k_2 v_o'} \quad (20)$$

To show that  $u_{eq}$  takes value in the interval of 0 to 1 in the sliding surface, the inequality of Equation (19) must be used. This is transformed to Equation (21) after reaching time ( $\delta(t)|_{t>0^+} = 0$ ):

$$La_3 \frac{i_L}{C} < a_1 E + La_4(v_o - V_d) + La_3 \frac{i_L}{C} - La_3 \frac{v_o}{RC} < a_1 v_o + a_2 \frac{i_L}{C} - a_2 \frac{v_o}{RC} \rightarrow 0 < La_3 \frac{i_L}{C} < a_1 E + La_4(v_o - V_d) + La_3 v_o' < a_1 v_o + a_2 v_o' \quad (21)$$

Dividing both sides of the inequality (21) by  $L(a_1 v_o + a_2 v_o') > 0$ . Then, it is given that  $0 < 1 - u_{eq} < 1$  or  $0 < u_{eq} < 1$ . Replacing  $u_{eq}$  into the voltage equation of (5), it yields:

$$Ri_L = \frac{(RCv_o' + v_o)(k_1 v_o + k_2 v_o')}{k_1 E + a_3 v_o' + a_4(v_o - V_d)} \quad (22)$$

$i_L$  contains the time derivative of the current error and integral term of the voltage error. It is obtained from  $S \approx 0$  as:

$$i_L = \frac{a_1 I_d - a_3 e - a_4 \int e}{a_1 + a_2 d/dt} \quad (23)$$

where  $e = (v_o - V_d)$ . With  $v_o' = e'$ ,  $v_o'' = e''$  and substituting (23) to (22), yields:

$$R(a_1 I_d - a_3 e - a_4 \int e) = a_1 \frac{(RCe' + e + V_d)(k_1 e + k_1 V_d + k_2 e')}{k_1 E + a_3 e' + a_4 e} + a_2 [(RCe'' + e')(k_1 e + k_1 V_d + k_2 e') + (RCe' + e + v_d)(k_1 e' + k_2 e'')] [k_1 E + a_3 e' + a_4 e] - (RCe' + e + V_d)(k_1 e + k_1 V_d + k_2 e')(a_3 e'' + a_4 e') / (k_1 E + a_3 e' + a_4 e)^2 \quad (24)$$

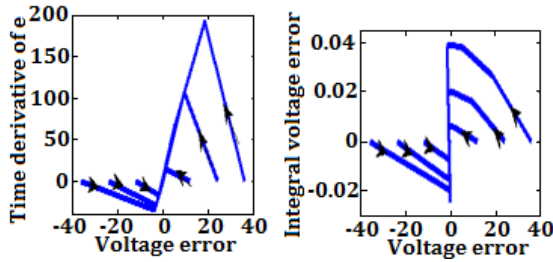


Figure 3. Phase portrait of the closed loop system around origin

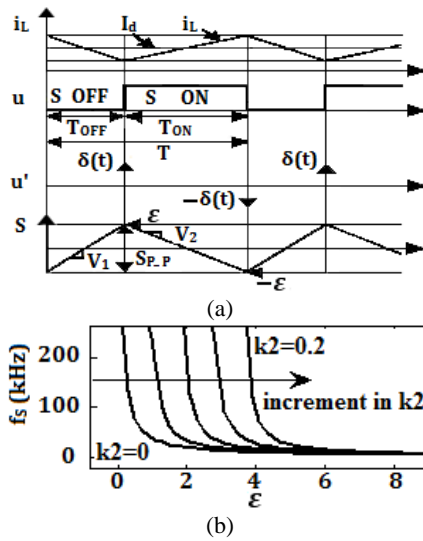


Figure 4. (a) Waveforms of the inductor current, switching pulse, time derivative of the control law and sliding surface in steady phase during the switching operation of the SMC; (b) Theoretical switching frequency of the designed SMC

TABLE 1. The parameters of the NOLC

Parameter	Symbol	Value
Input voltage	E	12 V
Nominal output voltage	$V_o$	36 V
Inductor	L	110 $\mu$ H
Capacitor	$C_1, C_2$	100 $\mu$ F
Nominal load resistance	R	50 $\Omega$

Consider three state variables be  $z_1 = \int e$ ,  $z_2 = e$ ,  $z_3 = e'$ . Then,  $z_1' = f_1(z_1, z_2, z_3) = z_2$ ,  $z_2' = f_2(z_1, z_2, z_3) = z_3$  and  $z_3' = f_3(z_1, z_2, z_3) = e''$ . The third function can be determined from Equation (24) as follows:

$$f_3(z_1, z_2, z_3) = [R(a_1 I_d - a_3 z_2 - a_4 z_1)(k_1 E + a_3 z_3 + a_4 z_2)^2 - a_1 (RCz_3 + z_2 + V_d)(k_1 z_2 + k_1 V_d + k_2 z_3)(k_1 E + a_3 z_3 + a_4 z_2) - a_2 (z_3(k_1 z_2 + k_1 V_d + k_2 z_3) + (RCz_3 + z_2 + v_d)k_1 z_3) [k_1 E + a_3 z_3 + a_4 z_2] - (RCz_3 + z_2 + V_d)(k_1 z_2 + k_1 V_d + k_2 z_3)a_4 z_3] / (a_2 [RC(k_1 z_2 + k_1 V_d + k_2 z_3) + (RCz_3 + z_2 + V_d)k_2] (k_1 E + a_3 z_3 + a_4 z_2) - a_3 (k_1 z_2 + k_1 V_d + k_2 z_3)(RCz_3 + z_2 + V_d)) \quad (25)$$

We define  $(p_1, p_2, p_3)$  as the equilibrium point of the obtained system. At this point,  $p_1' = p_2' = p_3' = 0$ , with:

$$f_1(z_1, z_2, z_3) = f_2(z_1, z_2, z_3) = f_3(z_1, z_2, z_3) = 0 \quad (26)$$

Solving (26),  $p_2 = p_3 = 0$  and also:

$$p_1 = \frac{a_1}{a_4} (I_d - \frac{V_d^2}{RE}) \quad (27)$$

Therefore, there is an equilibrium point  $(\frac{a_1}{a_4} (I_d - \frac{V_d^2}{RE}), 0, 0)$  for the closed loop error system. If the origin is a hyperbolic equilibrium point, the trajectories of a nonlinear system in a small region of neighborhood of an equilibrium point is close to the trajectories of its linearization in this region [18]. Proper selection of the PD-PI parameters ensures that the equilibrium point  $(\frac{a_1}{a_4} (I_d - \frac{V_d^2}{RE}), 0, 0)$  is hyperbolic. The Jacobian matrix of the system around its equilibrium point is as follows:

$$A_1 = \begin{bmatrix} a_{11} & a_{12} & a_{13} \\ a_{21} & a_{22} & a_{23} \\ a_{31} & a_{32} & a_{33} \end{bmatrix}, B_1 = \begin{bmatrix} b_{11} & b_{12} \\ b_{21} & b_{22} \\ b_{31} & b_{32} \end{bmatrix} \quad (28)$$

where:

$$a_{11} = a_{13} = a_{21} = a_{22} = 0, a_{12} = a_{23} = 1, a_{31} = \frac{R a_4 (k_1 E)^2}{R a_4 (k_1 E)^2}, a_{32} = \frac{a_3 k_1 V_d^2 - a_2 [RCk_1 V_d + k_2 V_d] k_1 E'}{a_2 [RCk_1 V_d + k_2 V_d] k_1 E - a_3 k_1 V_d^2}, a_{33} = \frac{-R a_3 k_1^2 E^2 + a_4 k_1 a_1 V_d^2 - 2 a_1 k_1^2 E V_d}{a_2 [RCk_1 V_d + k_2 V_d] k_1 E - a_3 k_1 V_d^2} \cdot a_{33} = \frac{2 R k_1 a_3 a_1^2 I_d^2 E - a_1 R C k_1^2 E V_d - a_1 k_1 k_2 E V_d - a_1 a_3 k_1 V_d^2 - 2 a_2 k_1^2 E V_d^2 + a_2 a_4 k_1 V_d^2}{a_2 [RCk_1 V_d + k_2 V_d] k_1 E - a_3 k_1 V_d^2} \quad (29)$$

$$b_{11} = b_{12} = b_{21} = b_{22} = 0, b_{31} = \frac{R a_1 (k_1 E)^2}{R a_1 (k_1 E)^2}, b_{32} = \frac{[a_2 (RCk_1 V_d + k_2 V_d) k_1 E - a_3 k_1 V_d^2] - [-2 a_1 k_1^2 E V_d]}{a_2 (RCk_1 V_d + k_2 V_d) k_1 E - a_3 k_1 V_d^2}$$

and also:

$$\begin{bmatrix} \dot{z}_1 \\ \dot{z}_2 \\ \dot{z}_3 \end{bmatrix} = A_1 \begin{bmatrix} z_1 \\ z_2 \\ z_3 \end{bmatrix} + B_1 \begin{bmatrix} I_d \\ V_d \end{bmatrix} \quad (30)$$

where  $\tilde{z}_1, \tilde{z}_2, \tilde{z}_3, \tilde{I}_d$  and  $\tilde{V}_d$  are the perturbations of  $z_1, z_2, z_3, I_d$  and  $V_d$ . Consider the desired eigenvalues of the proposed system to be  $\lambda_1^*, \lambda_2^*$  and  $\lambda_3^*$ . By using the pole placement, it is given:

$$\begin{vmatrix} s - a_{11} & -a_{12} & -a_{13} \\ -a_{21} & s - a_{22} & -a_{23} \\ -a_{31} & -a_{32} & s - a_{33} \end{vmatrix} = (s - \lambda_1^*)(s - \lambda_2^*)(s - \lambda_3^*) \quad (31)$$

The system parameters are shown in Table 1. By using (31), the controller parameters can be determined as follows:

$$a_1 = 1, k_2 = 0.2, a_3 = 0.72, a_4 = 140 \quad (32)$$

From Equation (25), it is concluded that the system has a discontinuous subspace. It is  $(z_1, -V_d, 0)$  where  $z_1$  is any real point. Also, consider  $I_d = \frac{V_d^2}{RE}$ . Figure 3 shows the phase portrait of the SMCC around  $(0,0,0)$ . It is obviously understood that the equilibrium point is a stable node and it has a large attraction region. For all the initial points starting at  $[z_1(0), z_2(0), z_3(0)]$  with  $z_2(0) > -V_d$ , all the trajectories converge to origin. Therefore, it is found that the error dynamics of the closed loop system around the origin is at least semi globally stable with a large attraction region. The aforementioned phase portrait is for  $S = 0$ . However, in practice, the voltage error will converge to a small layer around the desired output voltage. Therefore, the error variables oscillate around 0.

Due to the property of the integral term, interior term of the integrator should be zero. Therefore, the voltage error approaches to zero. Furthermore, by integrating the voltage error from zero time to settling time, the inductor current reference can be calculated. By reaching the sliding variable and voltage error to zero, the inductor current reaches to its generated reference. It is noticed that the internal dynamic (voltage of the middle capacitor) is limited between 0 V and input voltage. Therefore, this internal dynamic is always bounded.

### 2. 3. The Switching Frequency Analysis

According to the converter operation, it is supposed that three terms on the right side of Equation (10) are very small compared with other terms. Moreover,  $u$  is a step function. Thus,  $u'$  is the Dirac delta function. When  $u$  steps up from 0 to 1,  $u' = \delta(t)$  and when  $u$  steps down from 1 to 0,  $u' = -\delta(t)$ . The time derivative of  $S$  during the switch-OFF and switch-ON is:

$$\begin{cases} V_1 = \frac{ds}{dt} |_{u=1} = k_1 E + k_2 \delta(t) v_o - a_3 \frac{v_o}{RC} = \frac{S_{p-p}}{T_{on}} > 0 \\ V_2 = \frac{ds}{dt} |_{u=0} = k_1 E - k_1 v_o - k_2 \delta(t) v_o + \left(\frac{a_3}{C} + k_2\right) i_L \\ \quad - \left(\frac{a_3}{C} + k_2\right) \frac{v_o}{R} = \frac{-S_{p-p}}{T_{off}} < 0 \end{cases} \quad (33)$$

where  $S_{p-p}$  is the hysteresis bandwidth of the controller comparator. Also,  $T_{on}$  and  $T_{off}$  are the ON and OFF time

intervals in a time period of the switching operation, respectively.  $V_1$  and  $V_2$  are the speed of the designed sliding variable in the two states. The switching operation of the SMC and waveforms of  $i_L, u, u'$  and  $S$  are shown in Figure 4a.  $S$  oscillates between  $-\epsilon$  and  $\epsilon$  by a hysteresis controller with speed of  $V_1$  in ON state and speed of  $V_2$  in OFF state around zero; i.e.,

$$S_{p-p} = 2\epsilon \quad (34)$$

From Equation (33), it is concluded that the speed of  $S$  is dependent on the Dirac delta function in both ON and OFF modes. From both theoretical and practical point of view, it is understood that the sliding surface is moved between  $-\epsilon$  and  $\epsilon$  with infinite speed. Therefore, the high frequency operation can be achieved. By using Equation (33), the average value of  $V_1$  and  $V_2$  are given as follows:

$$\begin{cases} \langle V_1 \rangle = k_1 E + k_2 V_d \frac{1}{T_{on}} - a_3 \frac{V_d}{RC} = k_1 E + k_2 V_d \frac{f_s}{D} - a_3 \frac{V_d}{RC} \\ \langle V_2 \rangle = k_1 E - k_1 V_d - k_2 V_d \frac{1}{T_{off}} + \left(\frac{a_3}{C} + k_2\right) \left(I_d - \frac{V_d}{R}\right) \\ = k_1 E - k_1 V_d - k_2 V_d \frac{f_s}{(1-D)} + \left(\frac{a_3}{C} + k_2\right) \left(I_d - \frac{V_d}{R}\right) \end{cases} \quad (35)$$

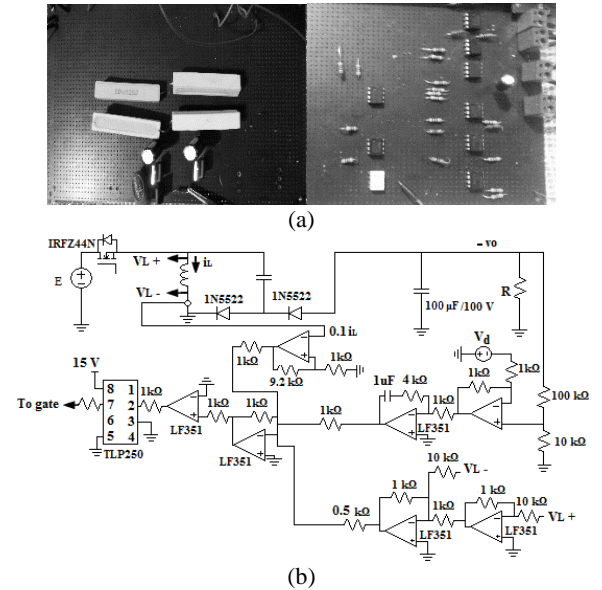


Figure 5. The structure of the developed system; (a) the setup of the system; (b) schematic diagram of the controller

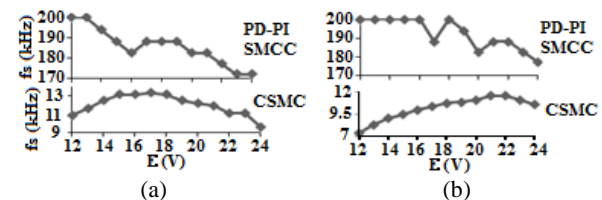


Figure 6. The practical switching frequency with the proposed PD-PI SMC and conventional strategy for  $V_o=36V$  and different input voltages; (a)  $R=100\Omega$ ; (b)  $R=50\Omega$ ;

where  $f_s$  is the switching frequency and  $D$  is the duty cycle of the converter, i.e.:

$$D = \frac{T_{on}}{T_{on}+T_{off}} = \frac{V_d-E}{V_d} \tag{36}$$

By using Equations (34)-(36), the switching frequency of the proposed SMC can be obtained as follows:

$$f_s = \frac{1}{T_{on}+T_{off}} = \frac{1}{\frac{2\varepsilon}{\langle V_1 \rangle} - \frac{2\varepsilon}{\langle V_2 \rangle}} = \frac{1}{\frac{2\varepsilon}{k_1 E + \frac{k_2 V_d^2}{V_d - E} f_s - a_3 \frac{V_d}{RC}} - \frac{2\varepsilon}{k_1 E - k_1 V_d - \frac{k_2 V_d^2}{E} f_s + (\frac{a_3}{C} + k_2)(I_d - \frac{V_d}{R})}} \tag{37}$$

Here, the switching frequency must be numerically obtained. We define  $\varepsilon_C$  as a critical hysteresis bandwidth in CCM. If  $\varepsilon < \varepsilon_C$ , the switching frequency converges to infinite. If the frequency largely increases, then  $\frac{k_2 v_d^2}{v_d - E} f_s \gg (k_1 E - a_3 \frac{V_d}{RC})$  and  $\frac{k_2 v_d^2}{E} f_s \gg (k_1 V_d - k_1 E + (\frac{a_3}{C} + k_2)(I_d - \frac{V_d}{R}))$ . By using Equation (37) and these assumptions,  $\varepsilon_C$  can be determined as follows:

$$\varepsilon_C = \frac{k_2 V_d}{2} \tag{38}$$

The switching frequency is shown in Figure 4. It is obvious that the coefficient  $k_2$  largely impacts on the frequency. If this parameter increases, then  $\varepsilon_C$  will effectively increase. Therefore, high switching frequency is achieved when there exists a large time delay or hysteresis bandwidth in practice. To construct derivative of the current for the defined sliding variable as shown in Figure 1, this paper uses the following relationship:

$$a_1 \frac{di_L}{dt} = k_2 v_L \tag{39}$$

#### 4. PRACTICAL RESULTS

An experimental set-up of the developed system was constructed. Figure 5a shows the photograph of the NOLC with the designed PD-PI based SMC. IRFZ44N and MBR20150C are selected as power switch and diodes. Also, three parallel inductors with ferrite cores and the value of 110  $\mu$ H/9A and two electrolytic capacitors with the value of 100  $\mu$ F/100 V are used for power converter. The current is measured using the ACS712-20A sensor and voltage measurement is done applying the resistive dividers. The photograph of the NOLC with the controller is shown in Figure 5b. In this work, the low slew rate OP-AMP LF351 is used for the signal amplification and hysteresis modulation to show the efficacy of the proposed controller for the switching frequency enhancement. In order to show the system robustness, the desired inductor current is disabled. Furthermore, the Rigol oscilloscope is used to save the practical tests and WFM Viewer software is used to show the obtained results in computer.

Figures 6a, b show the measured switching frequency with the proposed approach and conventional SMC operated in CCM against line variations for  $R=100, 50 \Omega$ , respectively. From these figures, it is observed that the practical frequency increases from the interval (7 14) to (170 200) kHz. Also, the ratio of the switching frequency variations to the average value of the switching frequency of the PD-PI based SMC is less than conventional SMC for the aforementioned points.

Consider  $V_0=36V, R=100 \Omega$ . Figures 7a and b show the steady waveforms of the current and generated control pulse of the NOLC in CCM for  $E=24$  and  $E=18$  V, respectively. It is clear that the converter under the proposed SMCC can works in CCM at low voltage gains and light loads. Furthermore, the sliding variable of the developed SMCC for  $E=18V, V_0=36$  V and  $R=100 \Omega$  is depicted in Figure 7c. This figure shows that the hysteresis bandwidth is about 8V. This value is so large, because of the large time delays of the circuit components. Hence, the experimental frequency of the conventional SMC effectively decreases. Moreover, the bandwidth is asymmetrical in practice.

Consider  $V_d = 36$  V,  $E = 12$  V and  $R = 50 \Omega$ . The system starts from the initial points of  $V_0(0) = 0$  V and  $i_L(0) = 0$  A.

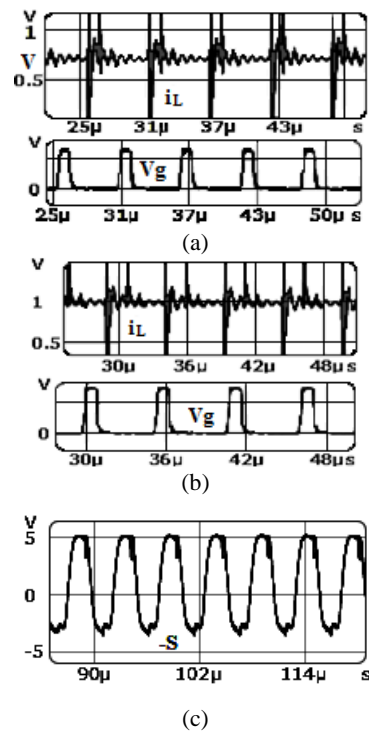


**Figure 7.** The steady performance of the system at low voltage gains; (a) inductor current and gate pulse waveforms for  $E=24$  V,  $R=100 \Omega$  and  $V_0=36$ ; (b) inductor current and gate pulse waveforms for  $E=18$  V,  $R=100 \Omega$  and  $V_0=36$ ; (c) the sliding variable for  $E=18$  V,  $V_0=36$  V and  $R=100 \Omega$

The practical result for this condition is shown in Figure 8a. In addition, Figure 8b illustrates the system response using the PD\_PI type SMCC for  $V_d = 36\text{ V}$ ,  $E = 15\text{ V}$  and  $R = 50\ \Omega$ .

Consider  $V_o=36\text{ V}$ . The load resistance steps-down from  $200$  to  $50\ \Omega$  and vice versa. Figures 9a and b depicts the system responses against load variation for  $E=12$  and  $18$ , respectively. In these figures, the voltage well follows its reference after the load change. Figure 10a shows the system response during transient region for  $R=100\ \Omega$ ,  $E=12\text{ V}$  and the voltage variation from about  $35$  to  $49\text{ V}$ . This figure demonstrates that the output variable has a good behavior. Also, the overshoot is  $1\text{ V}$  with settling time of about  $20\text{ ms}$ . Figure 10b shows the practical response for  $R=100\ \Omega$ ,  $E=12\text{ V}$  and the voltage change from about  $36$  to about  $22\text{ V}$ . For this test, the voltage overshoot equals to about  $6\text{ V}$  and settling time of about  $30\text{ ms}$ . Figure 11c depicts the voltage behavior for  $E=12\text{ V}$ ,  $R=36\ \Omega$  and voltage reference variation from nearly  $36$  to about  $22\text{ V}$ . For this experiment, the settling time is about  $40\text{ ms}$ .

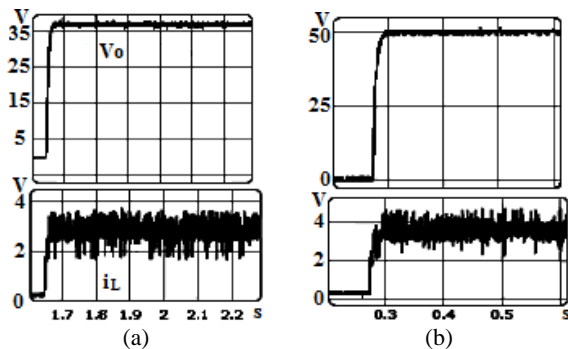


**Figure 8.** The transient response for  $R=50\ \Omega$ ;  $\Omega$  (a)  $V_o=36\text{ V}$ ,  $E=12\text{ V}$ ; (b)  $V_o=50\text{ V}$ ,  $E=18\text{ V}$

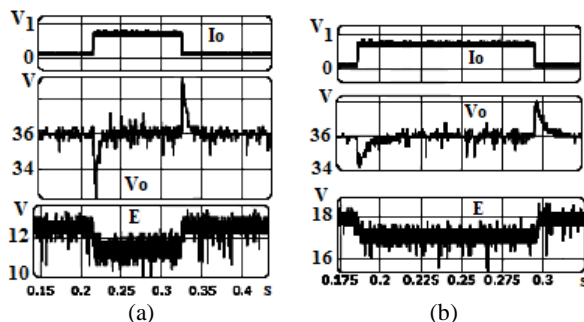


**Figure 9.** The practical results for load variation from  $200$  to  $50$  (a)  $E=12\text{ V}$ ,  $V_o = 36\text{ V}$ ; (b)  $E=18\text{ V}$ ,  $V_o = 36\text{ V}$

## 5. CONCLUSIONS

This study proposes a PD-PI type sliding mode current controller for a NOLC in CCM operation. A systematic

guideline for designing, developing and analyzing the characteristics of a cascade controller has been provided in the paper which includes proper choice of the sliding variable, investigation of the stability conditions and determination of the theoretical equation for the switching frequency. It is established that utilization of a PD compensator effectively enhances the switching frequency as compared with conventional sliding mode controller. By means of the suggested sliding variable, the minimum and maximum switching frequency increase from  $7$  and  $14\text{ kHz}$  to  $150$  and  $200\text{ kHz}$  for the aforementioned conditions, respectively. Furthermore, it is experimentally verified that the designed control scheme can well adjust the converter voltage with no steady error in presence of important disturbances in the uncertain parameters. It is said that the abrupt changes do not happen in practical applications at a same time. However, the practical experiments show high-accuracy trajectory tracking of the overall system for a strong system robustness and fast response against these abrupt variations.

## 6. REFERENCES

1. Prabhakar, M., "High gain dc-dc converter using active clamp circuit (research note)", *International Journal of Engineering-Transactions A: Basics*, Vol. 27, No. 1, (2013), 123-130.
2. Adell, P. C., Witulski, A. F., Schrimpf, R. D., Baronti, F., et al., "Digital control for radiation-Hardened switching converters in space", *IEEE Transactions on Aerospace and Electronic Systems*, Vol. 46, No. 2, (2010), 761-770.
3. Goudarzian, A., Nasiri, H., Abjadi, N., "Design and implementation of a constant frequency sliding mode controller for a Luo converter", *International Journal of Engineering-Transactions B: Applications*, Vol. 29, No. 2, (2016), 202-210.
4. Forouzesh, M., Siwakoti, Y., Gorji, A., Blaabjerg, F., Lehman, B., "Step-up dc/dc converters: a comprehensive review of voltage boosting techniques, topologies, and applications", *IEEE Transactions on Power Electronics*, Vol. 32, No. 12, (2017), 9143-9178.
5. Babu, R., Deepa, S., Jothivel, S., "A closed loop control of quadratic boost converter using PID-controller", *International Journal of Engineering-Transactions B: Applications*, Vol. 27, No. 11, (2014), 1653-1662.
6. Sarvi, M., Derakhshan, M., Sedighi Zade, M., "A new intelligent controller for parallel dc/dc converters", *International Journal of Engineering-Transactions B: Basics*, Vol. 27, No. 1, (2014), 131-142.
7. Suntio, T., "On dynamic modeling of PCM-controlled converters-buck converter as an example", *IEEE Transactions on Power Electronics*, Vol. 33, No. 6, (2017), 5502-5518.
8. Abjadi, N. R., Goudarzian, A. R., Arab Markadeh, Gh. R., Valipour, Z., "Reduced-order backstepping controller for POESLL DC/DC converter based on pulse width modulation", *Iranian Journal of Science and Technology, Transactions of Electrical Engineering*, (2018), To be published:doi.org/10.1007/s40998-018-0096-y(01)
9. Azadnia, A. H., Siah, A., Motameni, M., "An adaptive fuzzy neural network model for bankruptcy prediction of listed companies on the Tehran stock exchange. *International Journal*

- of Engineering-Transactions C: Aspects*, Vol. 30, No. 12 (2017) 1879-1884
10. Vali, M. H., Rezaie, B., Rahmani, Z., "Designing a neuro-sliding mode controller for networked control systems with packet dropout", *International Journal of Engineering-Transactions A: Basics*, Vol. 29, No. 4, (2016), 490-499.
  11. Goudarzian, A., Khosravi, A., "Design, analysis, and implementation of an integral terminal reduced-order sliding mode controller for a self-lift positive output Luo converter via Filippov's technique considering the effects of parametric resistances", *International Transactions on Electrical and Energy Systems*, (2018), e2776. <https://doi.org/10.1002/etep.2776>.
  12. Nasiri, H., Goudarzian, A., Pourbagher, R., Derakhshandeh, S. Y., "PI and PWM sliding mode control of POESLL converter", *IEEE Transactions on Aerospace and Electronic Systems*, Vol. 53, No. 5, (2017), 2167-2177.
  13. Qi, W., Li, S., Tan, S. C., Hui, S., "Parabolic-modulated sliding mode voltage control of buck converter", *IEEE Transactions on Industrial Electronics*, Vol. 65, No. 1, (2018), 844-854.
  14. Zhao, Y., Qiao, W., Ha, D., "A sliding mode duty ratio controller for dc/dc buck converters with constant power loads", *IEEE Transactions on Industrial Applications*, Vol. 50, No. 2, (2014), 1448-1458.
  15. Mamarelis, E., Petrone, G., Spagnuolo, G., "Design of a sliding-mode-controlled SEPIC for PV MPPT applications", *IEEE Transactions on Industrial Electronics*, Vol. 61, No. 7, (2014), 3387-3398.
  16. Vidal-Idiarte, E., Carrejo, C. E., Calvente, J., Martínez-Salamero, L., "Two-loop digital sliding mode control of dc/dc power converters based on predictive interpolation", *IEEE Transactions on Industrial Electronics*, Vol. 58, No. 6, (2011), 2491-2501.
  17. Bhat, S., Nagaraja, H. N., "DSP based proportional integral sliding mode controller for photo-voltaic system", *International Journal of Electrical Power & Energy Systems*, Vol. 71, (2015), 123-130.
  18. Knalil, H. K. *Nonlinear Systems*. Upper Saddle River, NJ: Prentice-Hall, (2002).

## Voltage Regulation of a Negative Output Luo Converter Using a PD-PI Type Sliding Mode Current Controller

A. Goudarzian, A. Khosravi

*Department of Electrical Engineering, Faculty of Engineering, Shahrekord Branch, Islamic Azad University, Shahrekord, Iran*

### P A P E R I N F O

چکیده

#### Paper history:

Received 19 September 2018

Received in revised form 19 November 2017

Accepted 03 January 2019

#### Keywords:

Switching Converter

Negative Output Luo Converter

PD-PI Type Sliding Surface

Control Design

این مقاله یک کنترل کننده مد لغزشی جدید نوع PD-PI برای مبدل NOLC در حالت هدایت پیوسته ارائه می دهد. بخاطر تغییرات بار و ولتاژ ورودی، دینامیک مبدل به شدت غیرخطی است. برای بهبود عملکرد مبدل و تنظیم جریان ورودی و ولتاژ خروجی مبدل، یک کنترلر غیرخطی نیاز است. کنترل کننده پیشنهادی متناسب با ذات پیچیده مبدل است. نتایج عملی نشان دهنده عملکرد بسیار خوب کنترلر پیشنهادی هستند که قادر است با حذف خطای دائم ولتاژ، مبدل را در بارهای بسیار سبک و فرکانس کلیدزنی بالا در نقاط کاری مختلف کنترل کند.

doi: 10.5829/ije.2019.32.02b.13